Journal of Computational Applied Mechanics 2023, 54(3): 410-424

DOI: 10.22059/JCAMECH.2023.364255.861

RESEARCH PAPER

Numerical Investigation of MHD Carreau Hybrid Nanofluid Flow over a Stretching Sheet in a Porous Medium with Viscosity Variations and Heat Transport

Hamzeh Taha Alkasasbeh*

Department of Mathematics, Faculty of Science, Ajloun National University, P.O. Box 43, Ajloun 26810, Jordan.

Abstract

This article delves into the interpretation of the Lorentz force's impact when employing the Carreau hybrid nanofluid model with infinite shear rate viscosity over a stretching sheet, which incorporates porous medium. This model is highly effective in elucidating various non-Newtonian fluid behaviors, encompassing shear thinning and thickening properties. The governing equations consist of coupled nonlinear PDEs, which are transformed into a set of coupled nonlinear ODEs using similarity transformations. These equations are then numerically solved using a MATLAB built-in solver (bvp4c). Different characteristics of the considered flow of various parameters, such as the magnetic parameter, porous media parameter, Weissenberg number, stretching parameter, ratio parameter, coefficients space, and heat source/sinks, on temperature and velocity profiles, which are presented graphically. Additionally, the impacts of these parameters on the skin-friction coefficient and Nusselt number are tabulated. The Key findings suggest that, the higher values of the porous media parameter, magnetic parameter, Weissenberg number, and stretching parameter led to a decrease in velocity by 67.12% and 75.49% on average. Moreover, the velocity profile, Nusselt number, and skin friction coefficient are higher for the Al_2O_3/KO-based nanofluid compared to the Al_2O_3+MoS_2/KO-based hybrid nanofluid. Also, the boundary layer of the hybrid nanofluid is observed to be hotter than that of the single nanoparticle nanofluid.

Keywords: Carreau Hybrid Nanofluid, MHD, (Bvp4c) Method, Stretching Sheet Porous Medium.;

1. Introduction

The remarkable ability of nanofluids to transfer heat in a wide variety of commercial and engineering applications has attracted a great deal of researchers' interest due to their high degree of versatility. Traditional fluids like water, ethylene glycol, and motor oil have poor thermal conduction, leading to inefficiency in modern cooling applications. Nanofluids, on the other hand, consist of minuscule particles such as copper, alumina, carbides, nitrides, metal oxides, graphite, and carbon nanotubes, which enhance the thermal conductivity of the base fluids. These nanoparticles typically have diameters ranging from 1 to 100 nm. By incorporating nanofluids into the cooling systems, their heat transfer capabilities are significantly improved, making them a promising solution for enhancing thermal performance in a wide range of practical applications. The concept of using nanoparticles to enhance the thermal conductivity and

* Corresponding author. Tel.: +962798662512.
E-mail address: alkasasbehh@gmail.com and alkasasbehh@anu.edu.jo

heat transfer rate of base fluids was first proposed by Choi [1]. In his pioneering work, titled "Enhancing Thermal Conductivity of Fluids with Nanoparticles," he demonstrated that the addition of nanoparticles to a base fluid could significantly improve its thermal conductivity and, consequently, its heat transfer capabilities. Choi's groundbreaking research laid the foundation for the development and exploration of nanofluids as a promising technology for efficient heat transfer in various applications. Since then, numerous researchers have further investigated and expanded upon the potential benefits and applications of nanofluids in the field of heat transfer. After evaluating the thermal conductivity of various metal oxides.

The research on nanofluids and their improved thermal conductivity has been significantly influenced by various studies conducted by different researchers. Lee et al. [2] found that both the shape and size of nanoparticles played a crucial role in enhancing the thermal conductivity of nanofluids. Subsequently, Buongiorno [3] investigated the parameters affecting nanofluid thermal conductivity and identified Brownian motion and the thermophoresis effect as factors contributing to the enhancement. Nield and Kuznetsov [4] applied Buongiorno's model to study the boundary layer stream, while Khan and Pop [5] conducted research on constant nanofluid flow over a stretched sheet. Makinde and Aziz [6] explored heat transfer properties of nanofluid flow using convective boundary conditions. Among various mathematical models, the Tiwari and Das models have become fundamental tools used in numerous published papers that investigate heat and mass transport in nanofluids [7-13]. These studies collectively contributed to a deeper understanding of nanofluids' heat transfer behaviour and opened up new possibilities for their practical applications in various fields.

Hybrid nanofluids can be considered as a new generation of Nanofluids. It is a very new idea. This is the composition of two variant types of dispersed nanoparticles in base fluids. This phenomenon have tale features that might make them helpful in many heat transfer organizations, like microelectronics, components of energy, pharmaceutical equipment, half breed powdered engines, engine cooling, car warming Administration, home cooler, chiller, thermal exchanger, atomic reactor coolant, grinding machinery, space innovation Choi and Eastman [14].

In recent research, several studies have been conducted to explore the properties and applications of hybrid nanofluids. Sundar [15] proposed a comprehensive method for producing hybrid nanofluids, discussing their advantages and disadvantages. Waini et al. [16] investigated the behaviour of a sheet-induced hybrid nanofluid created by adding copper nanoparticles to an Al_2O_3/water nanofluid, examining stretching and contracting effects. To understand the impact of various factors on heat and mass transfer in unsteady MHD flow over a stretched surface, Shreedevi et al. [17] combined carbon nanotubes and silver nanoparticles in the base fluid (water), considering thermal radiation, chemical reaction, suction, and slip conditions. Yashkun et al. [18] studied the influence of radiation and suction on the dynamics of an MHD hybrid nanofluid flowing over a stretching sheet, focusing on heat transfer. Their findings showed that the hybrid nanofluid (Cu + Al_2O_3/water) exhibited superior heat transfer characteristics compared to the conventional nanofluid (Cu/water). Rajesh et al. [19] analyzed the heat transfer processes of an unstable hybrid nanofluid flow across a flat vertical plate using an analytical approach. Additionally, Alkasasbeh [20] investigated the effects of heat transmission and MHD on the flow of a Casson hybrid nanofluid, which combined CuO and GO nanoparticles in methanol, over a vertically stretching sheet. Shaw et al. [21] offered a comprehensive analysis of hydromagnetic flow and thermal characteristics for Cross hybrid nanofluids, taking into account the influence of linear, nonlinear, and quadratic thermal radiations. Talebi et al. [22] introduced a study on the flow of a mixture-based dusty hybrid nanofluid in porous media, which was influenced by a magnetic field. They employed the radial basis function method for their analysis. Furthermore, several studies [23-28] have discussed the boundary layer flow and heat transfer characteristics of a hybrid micropolar nanofluid model over a solid sphere. These studies collectively contribute to our understanding of hybrid nanofluids and their potential for enhancing heat transfer processes in various applications.

The Carreau viscosity model is highly valuable in explaining the flow behaviour of fluids in regions with high shear rates, as it provides a relationship between viscosity and shear rate. This model was originally proposed by Carreau through a molecular network theory of rheology [29]. Studying boundary layer flow over stretching sheets has become increasingly important due to its relevance in various engineering and industrial applications. Researchers have paid significant attention to this subject. Industries involved in the production of paper, glass-fiber, solidification of liquid crystals, petroleum extraction, use of exotic lubricants, wire drawing for making suspensions, continuous cooling, fiber spinning, plastic film manufacturing, and polymer sheet extraction, among others, are particularly interested in this area [30]. The first study of a boundary layer flow past a stretching sheet was conducted by Crane [31]. Since then, researchers have continued to develop improved models and approaches to understand and describe the flow phenomenon. For instance, Zyphur et al. [32] developed a general cross-lagged panel model, which is an enhanced version utilizing a different approach. Ullah et al. [33] modelled the magnetic-Carreau nanofluid, considering the radiation effect, while Salahuddin [34] focused on modelling the Carreau fluid for a stretching cylinder. Additionally, Ayub et al. [35] presented a study on the MHD effect, incorporating the Carreau nanofluid model with infinite shear rate viscosity and thermal radiation. These studies contribute to a deeper understanding of

flow behaviour, especially in complex scenarios involving boundary layer flow, high shear rates, and special fluid models like the Carreau viscosity model, which have practical implications in various industrial processes and applications.

The primary aim of this study is to examine how a combination of a magnetic field, constant wall temperature, and suction effect influences the flow of a Carreau hybrid nanofluid over an upward stretching sheet embedded in a porous medium. The nanofluid used in the investigation is prepared initially by mixing Al_2O_3 nanoparticles with a volume fraction (ϕ_1=0.1) into the base fluid, resulting in the Al_2O_3/kerosene oil (KO) nanofluid. Subsequently, MoS_2 nanoparticles with a volume fraction (ϕ_2=0.1) are added to the Al_2O_3/KO nanofluid, creating the Al_2O_3 + MoS_2 /KO hybrid nanofluid.

To study the flow behaviour, the governing partial differential equations are transformed into ordinary differential equations using similarity transformations. The researchers then solve these equations numerically with the aid of a MATLAB built-in solver (bvp4c). In addition to analyzing the behaviour of the Al_2O_3/KO nanofluid, the study aims to conduct a comprehensive comparison between the hybrid nanofluid (Al_2O_3+MoS_2/KO) and the regular nanofluid (Al_2O_3/KO). By doing so, the researchers seek to gain insights into the flow characteristics and heat transfer behaviour of the hybrid nanofluid, particularly in the presence of a magnetic field, constant wall temperature, and suction effect. These conditions make the investigation relevant to various engineering and industrial applications where similar scenarios may arise. The findings from this study can provide valuable information for optimizing heat transfer processes in practical applications.

2. Nomenclature

b	body force
B_0	Magnetic Field Strength, *Wb*
Cf	Local Skin Friction Coefficient,
c_p	Specific Heat Capacity, $Jkg^{-1}K^{-1}$
C_s	Coefficients of Space
Λ	Variable Permeability of Porous Medium,
ℓ	Gradient of velocity
M	Magnetic Parameter
m	Stretching Parameter
n	Carreau fluid index
Nu	Nusselt Number
Pr	Prandtl Number
Q	Heat Flux, Wm^{-2}
Re	Local Reynolds Number.
S_p	Heat Source/Sinks
T	Temperature,
u_w	Variable Shrinking Velocity, Ms^{-1}
V_w	Variable Velocity of Suction/Injection, Ms^{-1}
u	Velocity Component Along *x*-axis, Ms^{-1}
v	Velocity Component along *Y*-axis, Ms^{-1}
we	Williamson Parameter
μ	Dynamic Viscosity, $Kgm^{-1}s^{-1}$
k	Kinematic Viscosity, M^2s^{-1}
ρ	Density, Kgm^{-3}
σ	Electrical Conductivity, $A^2s^3kg^{-1}m^{-3}$
ϖ	Stream Function, $Kgm^{-1}s^{-1}$
τ	Shear Rate, $Kgm^{-1}s^{-2}$
ϵ	Ratio Parameter
ϕ	Nanoparticle Volume Fraction
Subscripts	
f	base fluid
hnf	Hybrid Nanofluid
w	Wall/Surface
∞	Ambient Environment

3. Mathematical Formulation

In this problem, the flow of a Carreau hybrid nanofluid in steady state over a stretching sheet is been taken into consideration. The x-axis is considered along the stretching sheet and y-axis is taken perpendicular to stretching surface. Magnetic field is taken along the y-axis which is normal to the sheet surface and the flow is bounded by y > 0. Since the fluid's ambient temperature is assumed to be $T_w > T_\infty$, and the flow is initially moving at a nonlinear velocity of $U_w(x) = bx^m$, the parameter values $b,m > 0$ are connected to the stretching speed. The geometry of the fluid flow problem is presented in Fig 1. So, by assumption established, it is time to formulate the problem mathematically.

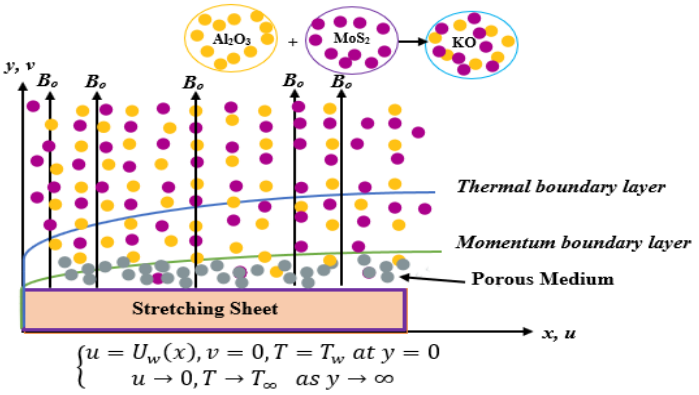

Fig 1: Geometry of the fluid problem.

The Mass, momentum, and energy, Equations of with body force b are see [35-37]

$$\nabla G = 0 \tag{1}$$

$$\rho \frac{dG}{dt} = div(\tau) + b \tag{2}$$

$$\rho C_p \frac{dT}{dt} = \tau L - divq \tag{3}$$

$$\tau = -pI + \mu(\omega)A \tag{4}$$

$$\mu(\omega) = \mu_0 \left[\epsilon + (1-\epsilon)(1+(\gamma\omega)^2)^{\frac{n-1}{2}}\right], \tag{5}$$

$$\epsilon = \frac{\mu_\infty}{\mu_0}, \tag{6}$$

$$A = \nabla G + (\nabla G)^T \tag{7}$$

$$G = [u(x,y), v(x,y), 0] \tag{8}$$

The momentum equation for a Carreau fluid is derived by using (5) and (4) in (2) with the body force acting as the Lorentz force, and the energy equation for a non-uniform heat sink source is produced by using (7) in (3). As a result, the mass, momentum, and energy equations are maintained below:

$$\frac{\partial u}{\partial x} + \frac{\partial v}{\partial y} = 0 \tag{9}$$

$$u\frac{\partial u}{\partial x} + v\frac{\partial v}{\partial y} = \frac{\mu_{hnf}}{\rho_{hnf}}\frac{\partial^2 u}{\partial y^2}\left[\epsilon + (1-\epsilon)\left(1+\left(\gamma\frac{\partial u}{\partial y}\right)^2\right)^{\frac{n-1}{2}}\right] - \frac{\mu_{hnf}}{\rho_{hnf}}\left(\gamma\frac{\partial u}{\partial y}\right)^2\left[1+\left(\gamma\frac{\partial u}{\partial y}\right)^2\right]^{\frac{n-3}{2}}\frac{\partial}{\partial y}\left(\frac{\partial u}{\partial y}\right)(1-\epsilon) - u\left[\frac{\sigma_{hnf}B_0^2}{\rho_{hnf}} + \frac{\mu_{hnf}}{\rho_{hnf}}\frac{1}{k_p}\right] \tag{10}$$

$$u\frac{\partial T}{\partial x} + v\frac{\partial T}{\partial y} = \frac{k_{hnf}}{(\rho C_p)_{hnf}}\frac{\partial^2 T}{\partial y^2} + \frac{Q'''}{(\rho C_p)_{hnf}} \tag{11}$$

With BCs

$$\begin{cases} u = U_w(x), v = 0, T = T_w \text{ at } y = 0 \\ u \to 0, T \to T_\infty \text{ as } y \to \infty \end{cases} \tag{12}$$

Table 1. Hybrid nanofluid (HF)and nanoparticle thermophysical characteristics [20]

Properties	HF
μ Viscosity	$\frac{\mu_{hnf}}{\mu_f} = \frac{1}{(1-\phi_1)^{2.5}(1-\phi_2)^{2.5}}$
ρ Density	$\frac{\rho_{hnf}}{\rho_f} = \left[(1-\phi_2)\left\{(1-\phi_1)\rho_f + \phi_1\frac{\rho_{s1}}{\rho_f}\right\}\right] + \phi_2\frac{\rho_{s2}}{\rho_f}$
(ρC_P) Heat capacity	$\frac{(\rho C_p)_{hnf}}{(\rho C_p)_f} = \left[(1-\phi_2)\left((1-\phi_1) + \frac{\phi_1(\rho C_p)_{s1}}{(\rho C_p)_f}\right) + \phi_2\frac{(\rho C_p)_{s2}}{(\rho C_p)_f}\right]$
K Thermal conductivity	$\frac{K_{hnf}}{K_f} = \frac{(K_{s2}+2K_{bf}) - 2\phi_2(K_{bf}-K_{s2})}{(K_{s2}+2K_{bf}) + \phi_2(K_{bf}-K_{s2})}$ where $\frac{\kappa_{bf}}{\kappa_f} = \left[\frac{(\kappa_{s1}+2\kappa_f) - 2\phi_1(\kappa_f-\kappa_{s1})}{(\kappa_{s1}+2\kappa_f) + \phi_1(\kappa_f-\kappa_{s1})}\right]$
σ Electrical conductivity	$\frac{\sigma_{hnf}}{\sigma_f} = \left[1 + \frac{3\phi_1\left(\sigma_1\phi_1 + \sigma_2\phi_2 - \sigma_{bf}(\phi_1+\phi_2)\right)}{(\sigma_1\phi_1+\sigma_2\phi_2+2\phi\sigma_{bf}) - \phi\sigma_{bf}\left((\sigma_1\phi_1+\sigma_2\phi_2) - \sigma_{bf}(\phi_1+\phi_2)\right)}\right]$

Carreau fluid depending on the shear rate τ, the Carreau fluid's viscosity is $\mu(\omega)$ and the tensor is. While n>1 moves Carreau fluids into the category of shear thickening, also known as dilatant fluids, and heat flux is revealed by the Carreau-model index, which is constrained in the range of $0 < n < 1$,, it reveals the nature of shear thinning or another name for pseudo-plastic fluids, and heat flux is $Q = -k(grad\ T)$, Gradient of velocity is $\ell = grad(v)$.

The Stefan Boltzmann constant and the non-uniform heat source, Q''', are mathematically described as see [35]

$$Q''' = \left(\frac{kU_W(x)}{xv_f}\right)\left[C_s(T_\infty)f'(\varsigma) + S_p(T-T_\infty)\right] \tag{13}$$

Coefficients of space and heat source/sinks are identified by the terms C_s and S_p, respectively, and these terms depend on temperature. The category of case $C_s > 0$ and $S_p > 0$ shows the absorption of heat internally when they behave as $C_s > 0$and $S_p < 0$, therefore using (13) and (12) in (11) we obtain.

$$u\frac{\partial T}{\partial x} + v\frac{\partial T}{\partial y} = \frac{k_{hnf}}{(\rho c_p)_{hnf}}\frac{\partial^2 T}{\partial y^2} + \frac{kU_W(x)}{xv_f(\rho C_p)_{hnf}}\left[C_s(T_\infty)f'(\varsigma) + S_p(T-T_\infty)\right] \tag{14}$$

Suitable and appropriate transformation are;

$$\varsigma = y\left[\frac{b(m+1)}{2v_f}x^{m-1}\right]^{\frac{1}{2}},\ \varpi(x,y,t) = y\left[\frac{2v_f b}{m+1}x^{m+1}\right]^{\frac{1}{2}}f(\varsigma),\ \theta(\varsigma) = \frac{T-T_\infty}{T_w-T_\infty} \tag{15}$$

Here, stream function ϖ is defined in term of velocity components. $\left(u = \frac{\partial \varpi}{\partial y}, v = -\frac{\partial \varpi}{\partial x}\right)$

Using all requirements in (10), (14) PDEs are transformed into following ODEs

$$\frac{\mu_{hnf}}{\rho_{hnf}}\left[\epsilon + (1-\epsilon)(1+n(we)^2(f''(\varsigma))^2)(1+(we)^2(f''(\varsigma))^2)^{\frac{n-3}{2}}\right]f'''(\varsigma) - \left[M\frac{\sigma_{hnf}/\sigma_f}{\rho_{hnf}/\rho_f} + \frac{\mu_{hnf}/\mu_f}{\rho_{hnf}/\rho_f}\Lambda\right]f'(\varsigma) - \left(\frac{2m}{m+1}\right)f'^2(\varsigma) + f(\varsigma)f''(\varsigma) \tag{16}$$

$$\frac{k_{hnf}/k_f}{(\rho c_p)_{hnf}/(\rho C_p)_f}\theta''(\varsigma) + \Pr f(\varsigma)\,\theta(\varsigma) + \left[C_s f'(\varsigma) + S_p\theta(\varsigma)\right] \tag{17}$$

BCs are

$$\begin{cases} f(0)=0, f'(0)=1, \theta(0)=1 \\ f'(\infty)\to 0 \; and \; \theta(\infty)\to 0 \end{cases} \tag{18}$$

where the governing parameters are written as mentioned below:

$M=\frac{2\sigma_f B_0^2}{\rho_f b(m+1)x^{m-1}}$ (Magnetic parameter), $\Lambda=\frac{v_f}{k_p b}$ (Porous media parameter),

$Pr=\frac{\mu_f(C_p)_f}{k_f}$ (Prandtl number), $we=\sqrt{\frac{b^3(m+1)\gamma^2 x^{3m-1}}{2v_f}}$ (Weissenberg number)

The skin friction and Nusselt number are defined as:

$$Cf=\left(\frac{\tau_w}{\rho_f U_w^2}\right)_{y=0} \quad \tau_w=\mu_{hnf}\frac{\partial u}{\partial y}\left[\epsilon+(1+\epsilon)\left(1+\left(\gamma\frac{\partial u}{\partial y}\right)^2\right)^{(n-1)/2}\right] \tag{19}$$

$$Nu=-\frac{xk_{hnf}}{k_f(T_w-T_\infty)}\left(\frac{\partial T}{\partial y}\right)_{y=0} \tag{20}$$

Putting their requirements in (19,21) so;

$$Re^{1/2}Cf=\frac{\mu_{hnf}}{\mu_f}\sqrt{\frac{1}{2}(m+1)}f''(0)\left[\epsilon+(1+\epsilon)[1-(wef''(0))^2]^{\frac{n-1}{2}}\right] \tag{21}$$

$$Re^{-1/2}Nu=-\frac{k_{hnf}}{k_f}\sqrt{\frac{m+1}{2}}\theta'(0) \tag{22}$$

Here Re is Reynolds number and defined as $Re=\frac{bx^{m+1}}{v_f}$.

4. Solution Methodology

The equations (16) and (17) of the non-linear ordinary differential equations with BCs (18) are numerically solved by bvp4c using MATLAB. Every differential equation solver starts by transforming the equations into a first-order system of equations.

Thus, we introduce the following substitutions:

$$\begin{cases} y_1=f, y_2=f', y_3=f'', yy_a=f''', \\ y_4=\theta, y_5=\theta', yy_b=\theta'' \end{cases} \tag{23}$$

Using the substitutions mentioned above, the Eqs. (16) and (17) are written as follows:

$$yy_a=\left[\frac{1}{\left(\frac{\mu_{hnf}}{\rho_{hnf}}\left[\epsilon+(1-\epsilon)\left(1+n(we^2y_3^2)\left(1+(we^2y_3^2)^{\frac{n-3}{2}}\right)\right)\right]\right)}\right]+\left(\frac{2m}{m+1}\right)y_2^2-y_2y_3-\left[M\frac{\sigma_{hnf}/\sigma_f}{\rho_{hnf}/\rho_f}+\frac{\mu_{hnf}/\mu_f}{\rho_{hnf}/\rho_f}\Lambda\right]y_2 \tag{24}$$

$$yy_b=-\frac{(\rho C_p)_{hnf}/(\rho C_p)_f}{k_{hnf}/k_f}\left(\Pr y_1 y_4+C_s y_2+S_p y_4\right) \tag{25}$$

Corresponding BCs (18) are converted as:

$$\begin{cases} y_1(0) \\ y_2(0)-1 \\ y_2(\infty) \\ y_4(0)-1 \\ y_4(\infty) \end{cases} \tag{26}$$

In order to resolve the BVP via MATLAB, bvp4c has only three points of view: an ODE function for calculating the residuals in the boundary conditions, and a structure to guess a mesh. It is exactly the same as MATLAB's IVP solvers when it comes to control of these ODEs. In this collocation formula, the interval of integration is divided into subintervals using a mesh of points.

The resulting transformation above with the suitable IVP are coded into MATLAB software to compute numerically.

5. MATLAB process for solution chart

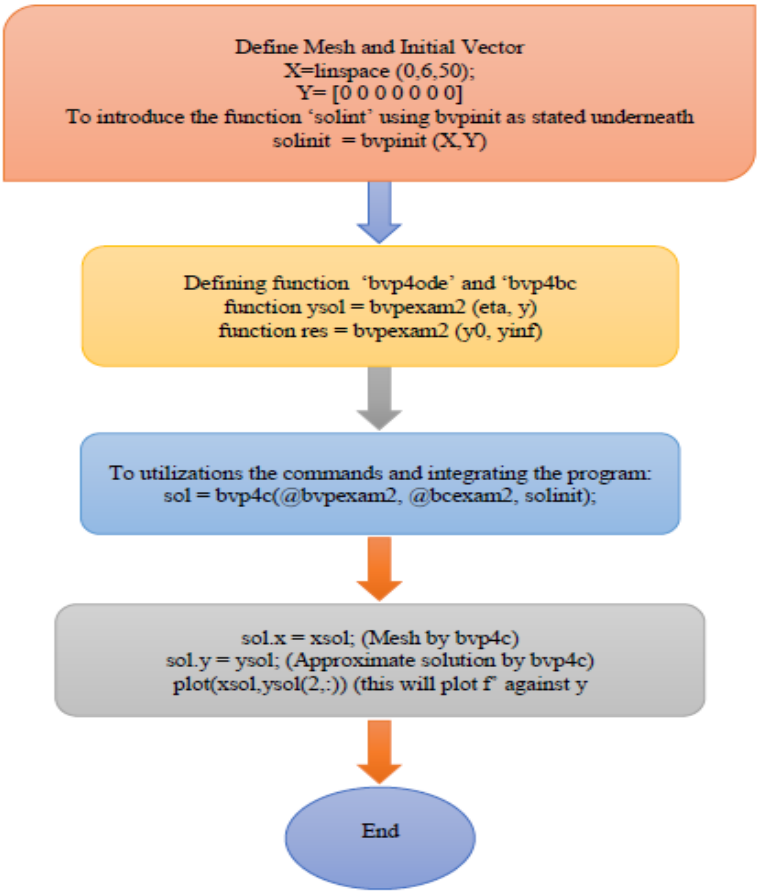

Fig 2: Flow chart of bvp4c method.

6. Results and Analysis

This section depicts the graphical effects of physical limitations on the velocity and temperature profiles of kerosene oil. -based Al_2O_3 and MoS_2 hybrid nanofluids as shown in Figs 3-14. Furthermore, the skin friction and Nusselt number rates for the nanofluids and hybrid nanofluids are calculated through Table 4. Table 2 displays the thermophysical properties. Table 3 represents the validation of the current outcomes with available literature which it in [36] and [37]. We noticed a good correlation between the outcomes from the past and the present. As a result, we vouch for the validity and veracity of the methodology used and the findings presented in this study.

Table 2: Thermo-physical properties of keroseone oil and metals nanoparticles [7, 11]

	$\rho(kgm^{-3})$	$C_p(Jkg^{-1}K^{-1})$	$k(Wm^{-1}K^{-1})$	$\sigma(Sm^{-1})$
Keroseone Oil	783	2090	0.145	6×10^{-10}
MoS_2	5060	397.21	904.21	2.09×10^{-9}
Al_2O_3	3970	523	25	1×10^{-10}

Table 3: Compared value $-\theta'(0)$ when n = 1and Pr = 1 with fixed value $we = \epsilon = M = C_s = S_p = \Lambda = \phi_1 = \phi_2 = 0$

m	Ref [36]	Ref [37]	Present study
0.2	0.610262	0.610202	0.610212
0.5	0.595277	0.595201	0.595211
1.5	0.574537	0.574730	0.574739
3	0.564472	0.564662	0.564664
10	0.554960	0.554951	0.554955

In Fig 3, the variation of velocity profiles with different porosity of the medium is shown. As the porous media parameter increases, it indicates that the flow occurs through a greater number of randomly oriented pores, leading to a reduction in the momentum boundary layer's thickness and velocity. The presence of porous media increases the contact surface area between the solid and liquid surface, influencing the flow characteristics.

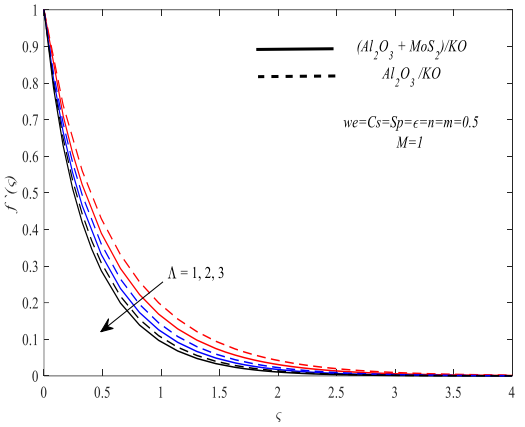

Fig 3: The effect of Λ on $f'(\varsigma)$

Fig 4 demonstrates the effect of the magnetic factor on velocity profiles. An increasing magnetic factor leads to a reduction in the velocity function. This is due to the magnetic force acting as an opposing force to fluid flow, resulting from the Lorentz force. Consequently, the magnetic force lowers the velocity of both fluids.

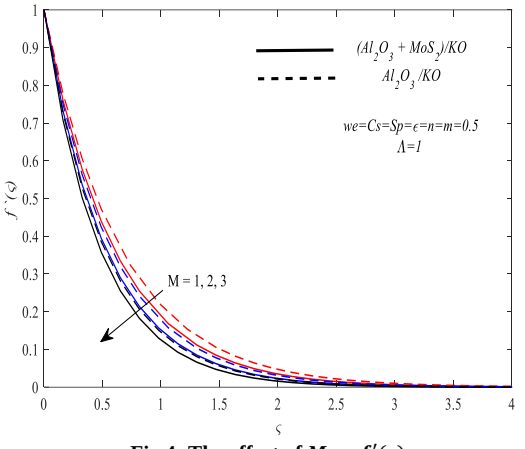

Fig 4: The effect of M on $f'(\varsigma)$

Fig 5 illustrates the impact of the Weissenberg number on velocity profiles. An increase in the Weissenberg number causes a decrement in fluid motion. Physically, this implies that a higher Weissenberg number leads to an increase in the fluid's elasticity, making the hybrid nanofluid and nanofluid more viscous. As a result, the fluid motion and the momentum boundary layer's thickness decrease for higher Weissenberg numbers.

In Fig 6, the influence of the ratio parameter (ϵ) on velocity profiles is shown. A greater ratio parameter increases the velocity. This effect is due to the increased ratio parameter reducing the length of the stretching sheet, resulting in a thinner momentum boundary layer. As a consequence, the influence of the boundary layer on the flow of both fluids is reduced, leading to an increase in the velocity profiles.

Fig 7 depicts the consequence of the stretching parameter (m) on velocity profiles. An increase in the stretching parameter reduces the velocity profiles. Higher values of the stretching parameter moderate the stretching rate of the sheet, leading to a decline in the velocity function.

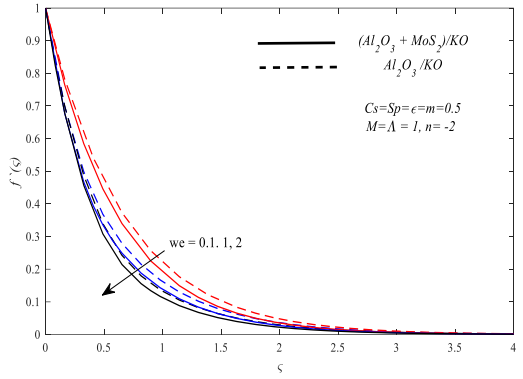

Fig 5: The effect of *(we)* on $f'(\varsigma)$

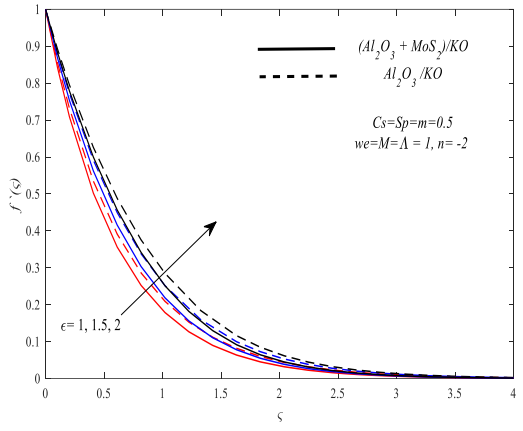

Fig 6: The effect of ϵ on $f'(\varsigma)$

Additionally, in all Figs, it is observed that the velocity of the nanofluid with Al_2O_3/KO is higher than the velocity of the hybrid nanofluid containing Al_2O_3+MoS_2/KO nanoparticles. This indicates that the presence of MoS_2 nanoparticles in the hybrid nanofluid leads to a reduction in velocity compared to the pure nanofluid containing only Al_2O_3/KO nanoparticles. This is likely due to the fact that the MoS_2 nanoparticles are heavier than Al_2O_3 nanoparticles see table 2.

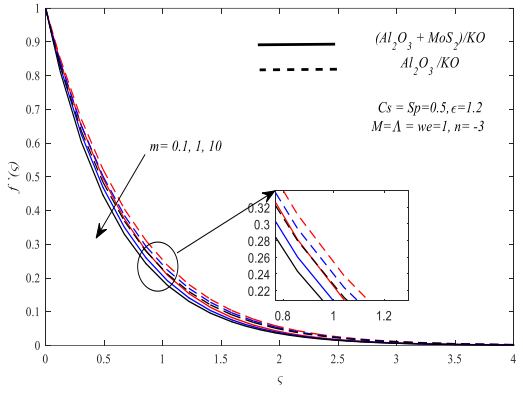

Fig. 7: The effect of m on $f'(\varsigma)$

In Fig 8, the temperature profiles for different porous medium parameters are shown. As the porous media parameter is increased from 1 to 3, the surface area of the porous media increases, leading to a rise in the temperature profile and thermal boundary layer.

Fig 9 illustrates the influence of the magnetic parameter (M) on temperature profiles. When the magnetic parameter increases, a resistant force occurs that competes with the fluid motion. As a result, heat is generated, and the volume fraction of boundary layer viscosity and thermal boundary layer viscosity become denser for a stronger magnetic

distribution. Therefore, the temperature increases with the increase of *M*.

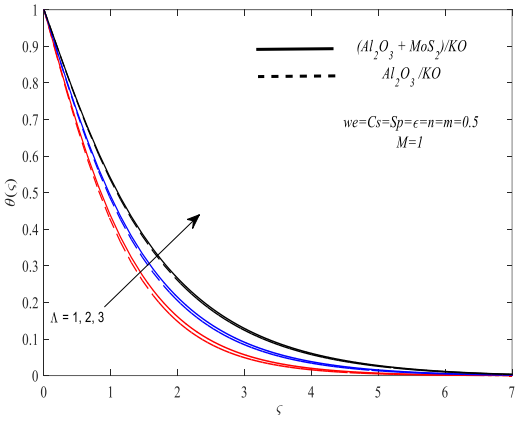

Fig 8: The effect of Λ on $\theta(\varsigma)$

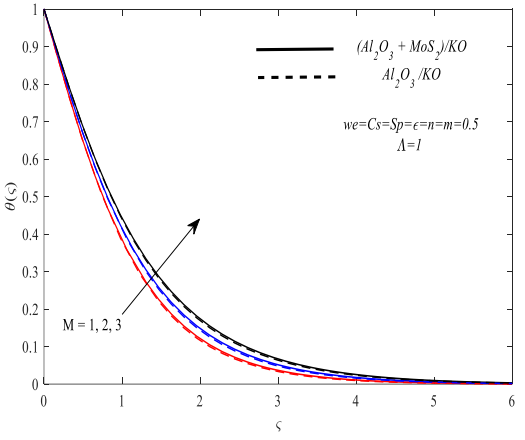

Fig 9: The effect of M on $\theta(\varsigma)$

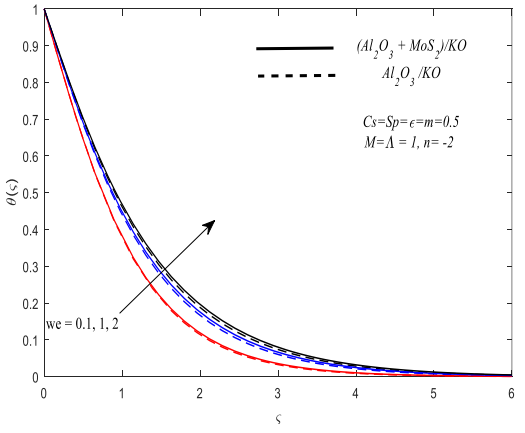

Fig 10: The effect of *(we)* on $\theta(\varsigma)$

From Fig 10, it is observed that an increase in the Weissenberg number (*we*) leads to a rise in the temperature. The improvement of temperature with the Weissenberg number indicates that higher Weissenberg numbers generate more heat, resulting in an enhanced temperature.

Fig 11 shows the impact of the ratio parameter (ϵ) on temperature profiles. It appears that the temperature decreases as ϵ increases. The variation in the temperature with the ratio parameter suggests that increasing ϵ reduces the length of the stretching sheet, leading to a thinner thermal boundary layer and lower temperatures.

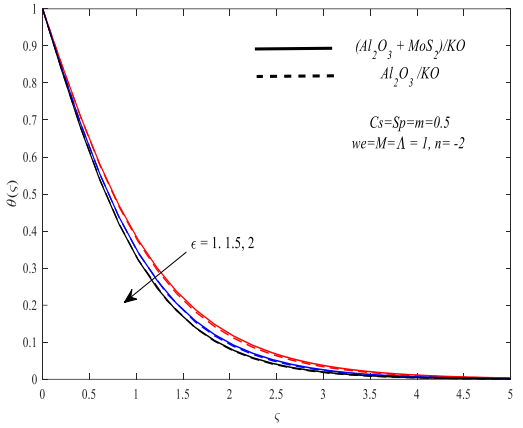

Fig 11: The effect of ϵ on $\theta(\varsigma)$

Figs 12 to 14 illustrate the impacts of coefficients space Cs, heat source/sinks (*Sp)*, and stretching parameter m on temperature profiles. The findings indicate that higher values of these physical parameters correspond to elevated temperatures. In particular, an increase in heat source/sinks (*Sp*) is associated with greater internal friction, leading to enhanced heat generation and a consequent rise in the thermal boundary layer, as demonstrated in Fig 13. Fig 14 reveals that the stretching parameter (*m*) exerts a positive influence on temperature, with a more pronounced effect observed for shear-thinned fluids. Furthermore, across all scenarios, the temperature of the Al_2O_3+MoS_2/KO hybrid nanofluid consistently exceeds that of the Al_2O_3/KO regular nanofluid, demonstrating that the hybrid nanofluid exhibits superior heat transfer characteristics in comparison.

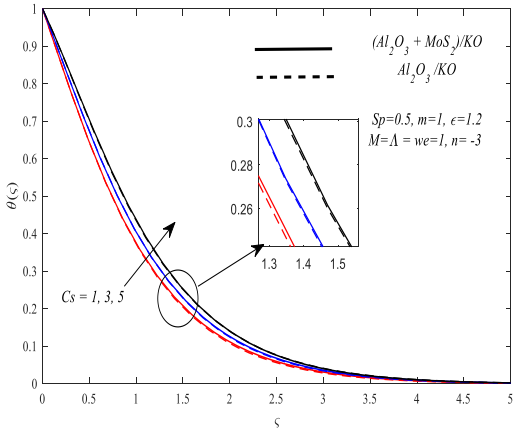

Fig 12: The effect of Cs on $\theta(\varsigma)$

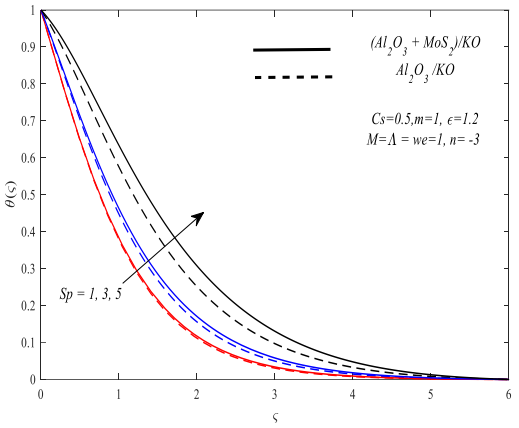

Fig13: The effect of Sp on $\theta(\varsigma)$

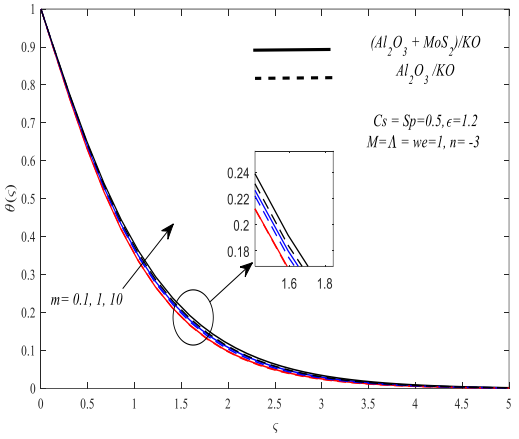

Fig14.: The effect of m on $\theta(\varsigma)$

Table 4. Description of $Re^{-1/2}Nu$ and $Re^{1/2}Cf$ for various value of different parameters

M	Λ	we	m	ϵ	C_s	S_p	$Re^{-1/2}Nu$		$Re^{1/2}Cf$	
							Hybrid nanofluid	Nanofluid	Hybrid nanofluid	Nanofluid
1	1	0.5	0.5	0.5	0.5	0.5	2.7592	2.9174	-3.0953	-1.5499
2							2.5947	2.7436	-17.5563	-3.4926
3							2.4530	2.5944	-	-143.4691
1	1	0.5	0.5	0.5	0.5	0.5	2.7592	2.9174	-3.0953	-1.5499
	2						2.5381	2.6636	-	-7.9882
	3						2.3570	2.4600	-	-
1	1	0.1	0.5	0.5	0.5	0.5	2.7862	2.9414	-1.0437	-0.7353
		1					2.7081	2.8694	-	-
		2					2.6299	2.7920	-	-
1	1	0.5	0.1	0.5	0.5	0.5	2.0643	2.1696	-1.5426	-0.9387
			1				3.6313	3.8541	-5.9083	-2.3941
			10				19.3868	20.7481	-339.1331	-20.6948
1	1	0.5	0.5	1	0.5	0.5	2.7875	2.9426	-1.0240	-0.7236
				1.5			2.8122	2.9647	-0.2833	-0.1884
				2			2.8341	2.9846	0.0944	0.1962
1	1	0.5	0.5	0.5	1		2.6679	2.8192	-3.0953	-1.5499
					3		2.3027	2.4264	-3.0953	-1.5499
					5		1.9375	2.0337	-3.0953	-1.5499
1	1	0.5	0.5	0.5	0.5	1	2.6087	2.7713	-3.0953	-1.5499
						3	1.8569	2.0654	-3.0953	-1.5499
						5	0.3814	0.8895	-3.0953	-1.5499

Table 4 presents the numerical values of important physical variables discovered during the investigation, including the skin friction coefficient ($Re^{1/2}Cf$) and the Nusselt number ($Re^{-1/2}Nu$) for different values of the

magnetic parameter (M), porous media parameter (Λ), Weissenberg number (we), stretching parameter (m), ratio parameter (ϵ), coefficients space (Cs), and heat source/sinks (Sp), for both the nanofluid and hybrid nanofluid. These quantities provide valuable insights into the effects of shear stress, heat transfer rate, and mass accumulation rate.

From the table, it is observed that the Nusselt number and skin friction coefficient decrease with increasing values of M, Λ, and we. On the other hand, their values increase with an increase in the ratio parameter (ϵ). Furthermore, the Nusselt number significantly increases with higher values of the stretching parameter (m), while the friction coefficient decreases considerably with the values of m.

Additionally, increasing values of the coefficients space (Cs) and heat source/sinks (Sp) lead to a reduction in the influence of the Nusselt number and stabilize the values of $Re^{1/2}Cf$

Comparing the performance between the nanofluid and the kerosene oil (KO)-based Carreau hybrid nanofluid, it is noted that the KO-based hybrid nanofluid has lower values compared to the water-based Carreau nanofluid. This can be explained by the fact that carbon nanotube nanoparticles have high thermal conductivity properties. The increased presence of carbon nanotube nanoparticles in the fluid enhances its thermal conductivity, making it more conductive and reducing its convective heat transfer capabilities.

Overall, the numerical values in Table 4 provide valuable insights into the effects of various physical parameters on the skin friction coefficient and Nusselt number for both the nanofluid and hybrid nanofluid, helping to understand the heat transfer and fluid flow behaviour in the investigated system.

7. Conclusion:

The current analysis was done to understand the flow characteristics and heat transfer in Carreau hybrid nanofluid near a stretching sheet with free convection and constant wall temperature. Several key parameters were investigated, including the magnetic parameter, porous media parameter, Weissenberg number, stretching parameter, ratio parameter, coefficients space, and heat source/sinks, under the influence of magnetohydrodynamic (MHD) effects. The governing partial differential equations were transformed into ordinary differential equations using similarity transformations, making the problem computationally tractable. The MATLAB bvp4c solver was utilized to numerically solve these equations. The obtained results were compared with published data, and an excellent agreement was observed, indicating the accuracy and reliability of the current analysis.

The significant findings are given below:

- A growth in the porous media parameter, magnetic parameter, Weissenberg number, and stretching parameter leads to a decline in velocity profiles. These parameters negatively influence the fluid motion, resulting in lower velocity profiles.
- An increase in the ratio parameter leads to an upsurge in velocity profiles. The ratio parameter positively impacts the fluid motion, leading to higher velocity profiles.
- The rise in the porous media parameter, magnetic parameter, Weissenberg number, stretching parameter, coefficients space, and heat source/sinks results in a growth in the temperature. These parameters contribute to increased heat generation and affect the temperature distribution in the flow.
- An increase in the ratio parameter leads to a decrease in the temperature. The ratio parameter reduces the length of the stretching sheet, resulting in a thinner thermal boundary layer and lower temperatures.
- The Nusselt number increases with the rise in the stretching parameter and ratio parameter, but it decreases with higher values of the porous media parameter, magnetic parameter, Weissenberg number, coefficients space, and heat source/sinks. These parameters influence the convective heat transfer capabilities and affect the Nusselt number.
- The skin friction coefficient declines for higher values of the porous media parameter, magnetic parameter, and stretching parameter, but it is lower for the ratio parameter. The skin friction coefficient characterizes the shear stress at the boundary and is affected by these influential parameters.
- The velocity profile, Nusselt number, and skin friction coefficient of the Al_2O_3/KO based nanofluid are higher than those of the Al_2O_3+MoS_2/KO based hybrid nanofluid. This indicates that the hybrid nanofluid exhibits better heat transfer and flow characteristics compared to the regular nanofluid.
- The boundary layer area of the hybrid nanofluid is observed to be hotter than that of the single nanoparticle nanofluid. The presence of MoS_2 nanoparticles in the hybrid nanofluid leads to increased heat generation and higher temperatures in the boundary layer.

Acknowledgement:

Author is grateful to acknowledge the Ajloun National University for providing the facilities support.

References

[1]. Choi, SU,JA Eastman. Enhancing thermal conductivity of fluids with nanoparticles. Argonne National Lab.(ANL), Argonne, IL (United States), 1995.
[2]. Lee, S, S-S Choi, S Li, and,J Eastman, Measuring thermal conductivity of fluids containing oxide nanoparticles, 1999.
[3]. Buongiorno, J, Convective transport in nanofluids, *Journal of Heat Transfer.* Vol 128, pp 240-250, 2006.
[4]. Kuznetsov, A,D Nield, Natural convective boundary-layer flow of a nanofluid past a vertical plate, *International Journal of Thermal Sciences,* Vol. 49, No. 2, pp. 243-7, 2010.
[5]. Khan, W,I Pop, Boundary-layer flow of a nanofluid past a stretching sheet, *International journal of heat and mass transfer,* Vol. 53, No. 11-12, pp. 2477-2483, 2010.
[6]. Makinde, OD,A Aziz, Boundary layer flow of a nanofluid past a stretching sheet with a convective boundary condition, *International Journal of Thermal Sciences,* Vol. 50, No. 7, pp. 1326-1332, 2011.
[7]. Alwawi, FA, HT Alkasasbeh, A Rashad,R Idris, MHD natural convection of Sodium Alginate Casson nanofluid over a solid sphere, *Results in physics,* Vol. 16, pp. 102818, 2020.
[8]. Swalmeh, MZ, HT Alkasasbeh, A Hussanan,M Mamat, Heat transfer flow of Cu-water and Al2O3-water micropolar nanofluids about a solid sphere in the presence of natural convection using Keller-box method, *Results in Physics,* Vol. 9, pp. 717-724, 2018.
[9]. Alkasasbeh, H, M Swalmeh, H Bani Saeed, F Al Faqih,A Talafha, Investigation on CNTs-water and human blood based Casson nanofluid flow over a stretching sheet under impact of magnetic field, *Frontiers in Heat and Mass Transfer (FHMT),* Vol. 14, pp. 1-10, 2020.
[10]. Alkasasbeh, HT, MZ Swalmeh, A Hussanan,M Mamat, Numerical solution of heat transfer flow in micropolar nanofluids with oxide nanoparticles in water and kerosene oil about a horizontal circular cylinder, *IAENG International Journal of Applied Mathematics,* Vol. 49, No. 3, pp. 1-8, 2019.
[11]. Alkasasbeh, HT, MZ Swalmeh, A Hussanan,M Mamat, Effects of mixed convection on methanol and kerosene oil based micropolar nanofluid containing oxide nanoparticles, *CFD Letters,* Vol. 11, No. 1, pp. 55-68, 2019.
[12]. Sen, S, M Das, M Nayak,O Makinde, Natural convection and heat transfer of micropolar hybrid nanofluid over horizontal, inclined and vertical thin needle with power-law varying boundary heating conditions, *Physica Scripta,* Vol. 98, No. 1, pp. 015206, 2022.
[13]. Hosseinzadeh, K, M Mardani, M Paikar, A Hasibi, T Tavangar, M Nimafar, D Ganji,MB Shafii, Investigation of second grade viscoelastic non-Newtonian nanofluid flow on the curve stretching surface in presence of MHD, *Results in Engineering,* Vol. 17, pp. 100838, 2023.
[14]. Lee, C, K Choi, R Leavitt,L Eastman, Infrared hot-electron transistor with a narrow bandpass filter for high temperature operation, *Applied physics letters,* Vol. 66, No. 1, pp. 90-102, 1995.
[15]. Sundar, LS, KV Sharma, MK Singh,A Sousa, Hybrid nanofluids preparation, thermal properties, heat transfer and friction factor–a review, *Renewable and Sustainable Energy Reviews,* Vol. 68, pp. 185-198, 2017.
[16]. Waini, I, A Ishak,I Pop, Unsteady flow and heat transfer past a stretching/shrinking sheet in a hybrid nanofluid, *International journal of heat and mass transfer,* Vol. 136, pp. 288-297, 2019.
[17]. Sreedevi, P, P Sudarsana Reddy,A Chamkha, Heat and mass transfer analysis of unsteady hybrid nanofluid flow over a stretching sheet with thermal radiation, *SN Applied Sciences,* Vol. 2, No. 7, pp. 1222-1234, 2020.
[18]. Yashkun, U, K Zaimi, NAA Bakar, A Ishak,I Pop, MHD hybrid nanofluid flow over a permeable stretching/shrinking sheet with thermal radiation effect, *International Journal of Numerical Methods for Heat & Fluid Flow,* Vol. 31, No. 3, pp. 1014-1031, 2020.
[19]. Rajesh, V, MA Sheremet,HF Öztop, Impact of hybrid nanofluids on MHD flow and heat transfer near a vertical plate with ramped wall temperature, *Case Studies in Thermal Engineering,* Vol. 28, pp. 101557, 2021.
[20]. Alkasasbeh, H, Numerical solution of heat transfer flow of casson hybrid nanofluid over vertical stretching sheet with magnetic field effect, *CFD Letters,* Vol. 14, No. 3, pp. 39-52, 2022.
[21]. Shaw, S, S Samantaray, A Misra, M Nayak,O Makinde, Hydromagnetic flow and thermal interpretations of Cross hybrid nanofluid influenced by linear, nonlinear and quadratic thermal radiations for any Prandtl number, *International Communications in Heat and Mass Transfer,* Vol. 130, pp. 105816, 2022.
[22]. Talebi Rostami, H, M Fallah Najafabadi, K Hosseinzadeh,D Ganji, Investigation of mixture-based dusty hybrid nanofluid flow in porous media affected by magnetic field using RBF method, *International Journal of Ambient Energy,* Vol. 43, No. 1, pp. 6425-6435, 2022.

[23]. Swalmeh, MZ, HT Alkasasbeh, A Hussanan, T Nguyen Thoi,M Mamat, Microstructure and inertial effects on natural convection micropolar nanofluid flow about a solid sphere, *International Journal of Ambient Energy*, Vol. 43, No. 1, pp. 666-677, 2022.

[24]. Alkasasbeh, H, Mathematical modeling of MHD flow of hybrid micropolar ferrofluids about a solid sphere, *Frontiers in Heat and Mass Transfer (FHMT)*, Vol. 18, pp. 1-10, 2022.

[25]. Alkasasbeh, HT, FM Al Faqih, Aa Alizadeh, MA Fazilati, H Zekri, D Toghraie, A Mourad, K Guedri,O Younis, Computational modeling of hybrid micropolar nanofluid flow over a solid sphere, *Journal of Magnetism and Magnetic Materials*, pp. 170444, 2023.

[26]. Upreti, H, AK Pandey, N Joshi,O Makinde, Thermodynamics and heat transfer analysis of magnetized Casson hybrid nanofluid flow via a Riga plate with thermal radiation, *Journal of Computational Biophysics and Chemistry*, Vol. 22, No. 03, pp. 321-334, 2023.

[27]. Alipour, N, B Jafari,K Hosseinzadeh, Optimization of wavy trapezoidal porous cavity containing mixture hybrid nanofluid (water/ethylene glycol Go–Al2O3) by response surface method, *Scientific Reports*, Vol. 13, No. 1, pp. 1635-1646, 2023.

[28]. Zangooee, M, K Hosseinzadeh,D Ganji, Hydrothermal analysis of hybrid nanofluid flow on a vertical plate by considering slip condition, *Theoretical and Applied Mechanics Letters*, Vol. 12, No. 5, pp. 100357, 2022.

[29]. Carreau, PJ, Rheological equations from molecular network theories, *Transactions of the Society of Rheology*, Vol. 16, No. 1, pp. 99-127, 1972.

[30]. Khan, M, H Sardar, MM Gulzar,AS Alshomrani, On multiple solutions of non-Newtonian Carreau fluid flow over an inclined shrinking sheet, *Results in physics*, Vol. 8, pp. 926-932, 2018.

[31]. Crane, LJ, Flow past a stretching plate, *Zeitschrift für angewandte Mathematik und Physik ZAMP*, Vol. 21, pp. 645-657, 1970.

[32]. Zyphur, MJ, PD Allison, L Tay, MC Voelkle, KJ Preacher, Z Zhang, EL Hamaker, A Shamsollahi, DC Pierides,P Koval, From data to causes I: Building a general cross-lagged panel model (GCLM), *Organizational Research Methods*, Vol. 23, No. 4, pp. 651-687, 2020.

[33]. Ullah, H, MI Khan,T Hayat, Modeling and analysis of megneto-Carreau fluid with radiative heat flux: Dual solutions about critical point, *Advances in Mechanical Engineering*, Vol. 12, No. 8, pp. 1687814020945477, 2020.

[34]. Salahuddin, T, Carreau fluid model towards a stretching cylinder: Using Keller box and shooting method, *Ain Shams Engineering Journal*, Vol. 11, No. 2, pp. 495-500, 2020.

[35]. Ayub, A, Z Sabir, SZH Shah, S Mahmoud, A Algarni, R Sadat,MR Ali, Aspects of infinite shear rate viscosity and heat transport of magnetized Carreau nanofluid, *The European Physical Journal Plus*, Vol. 137, No. 2, pp. 247-259, 2022.

[36]. Hamad, M,M Ferdows, Similarity solutions to viscous flow and heat transfer of nanofluid over nonlinearly stretching sheet, *Applied Mathematics and Mechanics*, Vol. 33, pp. 923-930, 2012.

[37]. Khan, M,Hashim, Boundary layer flow and heat transfer to Carreau fluid over a nonlinear stretching sheet, *AIP Advances*, Vol. 5, No. 10, pp. 107203, 2015.